Experimental and Thermodynamic Exploration of the High-Temperature Microstructures of Co-30 wt.% Cr-(2.5-5.0 wt.%) C Alloys

Patrice Berthod, Ophélie Hestin, Lionel Aranda, Thierry Schweitzer

▶ **To cite this version:**

Patrice Berthod, Ophélie Hestin, Lionel Aranda, Thierry Schweitzer. Experimental and Thermodynamic Exploration of the High-Temperature Microstructures of Co-30 wt.% Cr- (2.5-5.0 wt.%) C Alloys. Journal of Phase Equilibria and Diffusion, 2012, 33 (1), pp.29-39. 10.1007/s11669-011-9977-8 . hal-02534971

HAL Id: hal-02534971
https://hal.science/hal-02534971

Submitted on 7 Apr 2020

HAL is a multi-disciplinary open access archive for the deposit and dissemination of scientific research documents, whether they are published or not. The documents may come from teaching and research institutions in France or abroad, or from public or private research centers.

L'archive ouverte pluridisciplinaire **HAL**, est destinée au dépôt et à la diffusion de documents scientifiques de niveau recherche, publiés ou non, émanant des établissements d'enseignement et de recherche français ou étrangers, des laboratoires publics ou privés.

Experimental and Thermodynamic Exploration of the High-Temperature Microstructures of Co-30 wt.% Cr- (2.5–5.0 wt.%) C Alloys

Patrice Berthod, Ophélie Hestin, Lionel Aranda, Thierry Schweitzer

Institut Jean Lamour (UMR 7198), department CP2S
Faculty of Sciences and Technologies, UHP Nancy 1, Nancy - University
BP 70239, 54506 Vandoeuvre-lès-Nancy – France

Corresponding author's e-mail : pberthodcentralelille1987@orange.fr
Corresponding author's phone: (33)3 8368 4666 and fax number: (33)3 8368 4611

Pre-print de l'article **Journal of Phase Equilibria and Diffusion (2012) 33:29-39**
DOI: 10.1007/s11669-011-9977-8

Abstract

Cobalt alloyed with high contents in Cr and C potentially may lead to hard alloys candidate for high temperature applications involving wear degradations. The Co-30%wt-xC system was explored from x=2.5 to 5wt.% by both experiments and thermodynamic calculations. The stable microstructures at 1000, 1100 and 1200°C and the temperatures of solidus and liquidus were of interest. When the carbon content is between 2.5 and 3.5 the alloys display (hypo-)eutectic microstructures composed of FCC Co-based matrix and M_7C_3 carbides. Between 4 and 5wt.%C, the microstructures contain coarse pro-eutectic M_7C_3 carbides, leading to a total volume fraction of M_7C_3 close to 50% or higher. The C-richest alloys also contain graphite, instead cementite as predicted by calculations. A better agreement between experiments and calculations about microstructures and solidus temperature can be obtained by forbidding cementite in the calculation conditions. The obtained hardness level is about 650Hv but decreases when the heat-treatment temperature increases.

Keywords: Cobalt alloys; High carbon; Chromium Carbides; Graphite; Thermodynamic calculations; Hardness measurements

1. Introduction

Cobalt-based alloys containing several tens weight percents of chromium can be met in various domains. For example one can cite prosthetic dentistry [1], hot aeronautic/power generation components [2] and some of the fiberizing tools used in the glass industry [3]. Other cobalt alloys, not protected against wet or dry corrosion by such high chromium content, contain high quantities of carbon present as numerous carbides to take benefit of high hardness to resist wear; this is the case of cutting tools [4] made of a cobalt matrix containing high fractions of dispersed WC carbides, or wear-protective coatings [5] consisting in Co-W_2C deposited by thermal spray on steels. To achieve both wear resistance and corrosion resistance cobalt-based alloys can be alloyed with great quantities of carbon and chromium. This allows obtaining high

fractions of carbides acting first as efficient hardening particles bringing their high intrinsic hardness (much more than 1000 Hv [6]). Second these carbides may play the role of chromium reservoirs able to release this element when the alloy is in situation of oxidation to constitute and maintain the protective external chromia scale [7].

The oxidation resistance of such alloys is necessarily limited in time because of the impoverishment in chromium in the more external parts of the alloys, which leads sooner or later to the loss of their chromia-forming behaviour consecutively to the decrease of the surface Cr content under a critical value. In the same way a long exposure to high temperature may induce changes in nature, morphology and/or volume fraction for the carbides with consequently modifications of the hardness that they bring to the whole alloy. It is thus of importance to study how the microstructures of cobalt-based alloys can evolve morphologically and to know their stable state at the chosen temperature which describes the final natures and fractions of carbides.

The topic of this study is to enrich a previous one concerning heat-resistant chromium-rich ternary cobalt alloys containing up to 2wt.% of carbon [8], by considering higher carbon contents for the same {Co-30wt.%Cr} base. Similarly to what was done in this previous work, the goal is here to explore the high temperature metallurgical states of several alloys containing between 2.5 and 5wt.%C:

- by evaluating their refractoriness (which may be possibly lowered by too carbon),
- by characterizing the volume fractions of their carbides (probably higher and then potentially leading to higher hardnesses) and eventually discovering stoichiometry changes for C-richer ones,
- and possibly by discovering new phases rich in carbon potentially harmful for the hardness and the wear resistance.

2. Experimental details of the study

2.1. Elaboration and cutting of the alloys

Six alloys Co-30wt.% Cr-xC (x=2.5, 3.0, 3.5, 4.0, 4.5 and 5.0%wt), respectively named “Co25”, “Co30”, “Co35”, “Co40”, “Co45” and “Co50” with respect to their carbon contents, were synthesized by high frequency induction melting of pure cobalt, chromium and carbon (99.9%, Alfa Aesar) together. This was done using a CELES high frequency induction (300kHz) furnace and under an inert atmosphere of 300mbars of Argon to avoid oxidation of metals and loss of carbon. Fusion and solidification occurred in a copper crucible cooled by water circulation. The obtained ingots (all of about 40g) were cut in order to obtain, per alloy, a part for controlling the obtained microstructure (Scanning Electron Microscope Philips XL30) and chemical composition (CAMECA SX100 microprobe), three parts of about 0.25cm^3 for the exposures to high temperature and a smaller part (about 2 × 2 × 8mm^3) for the measurement of the solidus and liquidus temperatures.

2.2. High temperature exposures and metallographic characterization

The three samples for microstructure stabilization at high temperature were exposed for 50 hours in a tubular resistive furnace at 1000, 1100 and 1200 °C. These

temperatures were reached with a heating at about 20 °C/min and the cooling at the end of the 50h stage was done by air-quenching. The microstructures of the alloys were observed on metallographic samples. These ones were prepared by sectioning the alloy's samples after their aging at high temperature, using a Buehler Isomet 5000 precision saw. The two parts were embedded together in a mold using a cold resin system (Escil CY230 + HY956). They were polished using SiC paper from 120 to 1200 grid under water, and finally a textile enriched with 1µm hard particles.

X-Ray Diffraction experiments were performed using a Philips X'Pert Pro diffractometer (Cu Kα, 1.5406Å) to identify the present phases. A Scanning Electron Microscope (SEM, type: XL30 Philips) was used for the metallographic observations, essentially in the Back Scattered Electrons (BSE) mode and under an acceleration voltage of 20kV. The surface fractions of carbides were measured on three BSE micrographs (magnification × 1000) taken on each sample with the SEM in BSE mode, in three different locations randomly chosen near the middle of the initial ingot. The BSE detector leads to different levels of gray depending on the average atomic number of the considered phase: the pixels of matrix (gray) and chromium carbides (dark), and of graphite (black) when present, were then well separated. The Adobe Photoshop CS software was used on the three micrographs files of a same sample for measuring their surface fractions (supposed to be close to the volume fractions). The average value and the standard deviation (for assessing uncertainty) were then calculated.

The carbides volume fractions fv[Cr_xC_y] were deduced from the mass fractions fw[Cr_xC_y]) using equation the following equation:

$$f_v\left[Cr_xC_y\right] = \left(\frac{f_w\left[Cr_xC_y\right]}{\rho Cr_xC_y}\right) / \left(\frac{f_w\left[Cr_xC_y\right]}{\rho Cr_xC_y} + \frac{f_w\left[\text{matrix}\right]}{\rho_{\text{matrix}}}\right)$$

with 7.95 g cm^{-3} for the matrix (deduced from the weights and volumes of samples of binary Co-Cr alloys), 6.941 g cm^{-3} for the Cr_7C_3 carbides [9], and 2.25 g cm^{-3} for graphite.

2.3. Measurements of the temperature limits of the mushy states

The solidus and liquidus temperatures of the alloys were measured using Differential Thermal Analysis (DTA). The thermal cycle used was composed of a heating rate of 20 °C/min up to 1200 °C, followed by a slower heating at 5 °C/min up to 1500 °C for a better accuracy. Cooling was done first at 5 °C/min down to 1200°C, and second at 20 °C/min down to room temperature. Temperatures at beginnings and ends of fusion and solidification were measured. For the determination of the experimental solidus (resp. liquidus) the temperatures of start of fusion, of end of solidification and the average of the two previous ones (resp. end of fusion, start of solidification and the average of the two) were taken on consideration.

2.4. Thermodynamic calculations

In parallel, thermodynamic calculations were performed using the Thermo-Calc software [10], using a database containing the descriptions of the Co-Cr-C system and

its sub-systems [11-16]. Calculations were performed first for a qualitative purpose: comparison between the natures of the phases really obtained - visualized by SEM/BSE and identified by XRD - and those predicted by Thermo-Calc. This was done by computing phase diagrams, eventually with suspended phases. Secondly additional calculations were done for precise conditions sets to allow quantitative comparison between phase volume fractions (supposed equal to the surface fractions measured by image analysis) and volume fractions issued from the conversion of calculated mass fractions). Calculations were also achieved to obtain theoretic solidus and liquidus temperatures for comparison with those measured by DTA.

2.5. Hardness evaluation

The hardness of each alloy in all its heat-treated conditions was measured by Vickers indentations performed using a Testwell Wolpert apparatus. The applied load was 30kg. In each case several values were obtained, which led to average value and standard deviation used as uncertainty.

3. Results

3.1. Microstructures of the alloys in the as-cast conditions

The alloys obtained just after melting and solidification present very different microstructures following the carbon content (Fig. 1). The alloy containing 2.5wt.%C (Co25) contains dendrites of matrix and an interdendritic {matrix + carbide}- eutectic compound. This is also the case of the Co30 alloy which displays less numerous dendrites and more extended areas of eutectic compound, thanks to its higher carbon content. The microstructure of the Co35 alloy seems wholly eutectic. Several coarse acicular carbides, probably appeared at the first stage of solidification, are mixed with the eutectic matrix+carbide compound in the Co40 microstructure. These pro-eutectic carbides are both coarser and more numerous in the Co45 alloy. A new phase, extremely black when observed with the SEM in BSE mode, has appeared in the Co50 alloy in addition to the eutectic compound and the pro-eutectic carbides. This is seemingly graphite, since it is essentially composed of the lightest element in these alloys (carbon) and it presents features characteristic of the lamellar graphite wellknown in the gray cast irons).

3.2. Microstructures of the alloys after exposure at high temperature

Three parts of each alloy were thereafter exposed to 1000, 1100 or 1200°C for 50 hours, then metallographically prepared and observed with the SEM. The microstructures of these aged alloys are displayed in Fig. 2 for the Co25, Co30 and Co35 alloys, and in Fig. 3 for the Co40, Co45 and Co50 alloys. In all cases the microstructure of a same alloy does not really depend on the aging temperature and they seem to be almost unchanged by comparison with the as-cast microstructures. One can just notice a slight decrease in total carbide fraction when the considered temperature is higher, and a slight change of the carbides morphology after 50h at 1200°C (carbides a little more compact), essentially for the alloys with less than 4wt.%C.

More information was obtained about these microstructures after aging by performing X-Ray diffraction. All alloys for the three temperatures were analyzed and the obtained spectra obtained for selected alloys are given as examples in Fig. 4 (Co25), Fig. 5 (Co35) and Fig. 6 (Co45). It appears first that the matrix is composed of two types: Face Centered Cubic (FCC) and Hexagonal (HCP). In general the first allotropic type seems to be more present than the second one after an aging done at 1200°C, while it is on the contrary the HCP type which is the most present after aging at a lower temperature. A second observation concerns the type of carbide: there is seemingly only one type of chromium carbide present in all the alloys: Cr_7C_3. Thirdly, for the highest carbon contents, several additional peaks seem having appeared but they are very small. This led to difficulties for identifying them. To finish, the graphite phase, present in too small quantities, did not lead to any diffraction peaks.

3.4. Thermodynamic calculations

First thermodynamic calculations led to the 30Cr-section of the Co-Cr-2 to 5C phase diagram presented in Fig. 7(a). One find again that the alloys are hypo-eutectic for carbon contents lower than 3.5wt.%C. Their solidification starts with the matrix (dendrites seen in Fig.1 and Fig. 2 in the as-cast or aged microstructures of the Co25 and Co30 alloys). This is followed by a progressive precipitation of the {matrix+Cr_7C_3} eutectic, over a temperature interval increasing with the carbon content. The Co35 alloy effectively appears as a wholly eutectic alloy. Their stable microstructures are then composed of a FCC cobalt-based matrix and eutectic Cr_7C_3 carbides (more precisely $(Cr,Co)_7C_3$ carbides since a minor part of Cr is substituted by cobalt atoms in thes carbides according to Thermo-Calc). In contrast the solidification of the Co40, Co45 and Co50 alloys starts with the crystallization of pro-eutectic Cr_7C_3 carbides, and finishes with the precipitation of an matrix+carbides eutectic, with also the appearance of a new phase, cementite. In contrast, no graphite is predicted.

Considering that first graphite was experimentally obtained, and second that neither SEM observation nor X-Ray Diffraction has revealed the presence of cementite (although this phase seems stable at the three aging temperatures tested in this study), new calculations were performed with Thermo-Calc by obstructing the appearance of cementite (declared suspended phase). This led to a second pseudo-binary diagram (Fig. 7(b)), in which graphite has appeared and is present in the Co45 and Co50 alloys, as experimentally observed.

After the previous diagrams, calculations were performed for each alloy and each temperature of aging. In the case of the four C-richest alloys for which cementite appears according to Thermo-Calc, a second set of calculations was realized by suspending this cementite phase. All the obtained mass fractions are displayed in Table 1. Unsurprisingly an increase in carbon favors high mass fraction of Cr_7C_3 carbides and this fraction tends to slightly decrease when the aging temperature increases. This is true at least from 2.5%C to 3.5%C. Indeed, the appearance of cementite first slows the rise of Cr_7C_3 mass fraction with carbon between Co30 and Co35 and thereafter inverses the trend since the Cr_7C_3 quantity decreases because of a more rapid increase in cementite mass fraction. When cementite is suspended, the Cr_7C_3 mass fraction goes on increasing if the carbon content increases but this increase is much more limited than for the Co40 to Co50 alloys. Indeed, the greatest part of the additional carbon is then used to form supplementary graphite.

3.5. Quantitative comparisons between experiments and calculations

3.5.1. Phases' fractions

Considering that suspending cementite seems allowing thermodynamic calculations better represent reality, it was chosen to consider only the calculations done with this condition for the alloys from Co35 to Co50 (while this condition was not imposed for the alloys Co25 and Co30). The experimental results (phases' natures identified by SEM observations and XRD experiments, surface fractions measured by image analysis and assumed to be close to the volume fractions) and the calculated results (volume fractions issued from the conversion of the calculated mass fractions) are presented together in Table 2 for the three graphite-free alloys (Co25, Co30 and Co35) and in Table 3 for the three graphite-containing alloys (Co40, Co45 and Co50).

In general there is a good agreement between the two sets of values in Table 2 since either the calculated volume fractions belong to the interval of measured surface fractions, or is only just above or just below the interval limits. Just one mismatch can be noticed in the case of the Co30 alloy aged at 1100°C.

This good agreement remains for the Co40 alloy, for both Cr_7C_3 carbides and graphite which is not yet very present for 4wt.%C in the alloy. Unfortunately serious discrepancies start appearing when the carbon content reach the highest values (Co45 and Co50). Indeed there is a general trend to have for carbides experimental surface fractions higher than the calculated volume fractions and the inversed order concerning the graphite fractions (experimental values lower than calculated values).

3.5.2. Liquidus and solidus temperatures

The evolutions of the calculated liquidus and solidus temperatures were already shown above in the phase diagrams presented in Fig. 7. The DTA experiments led to heat flow curves on which the temperature of starts and ends of endothermic and exothermic phenomena were determined. The temperatures of fusion end on the heating part of the cyclic heat flux curve, of solidification start on the cooling part of the heat flux curve and their average value are graphically represented in Fig. 8(a). They are plotted together with the liquidus determined by Thermo-Calc without or with suspension of the cementite phase for the Co35 to Co50 alloys. In the same way the temperatures of fusion start on the heating part, solidification end on the cooling part and their average value are plotted in Fig. 8(b) with the ones calculated with Thermo-Calc for the same conditions.

The calculated results are consistent with the measurements for both liquidus and solidus for the Co25 to Co35 (maybe Co40 too) but severe discrepancies emerge for Co45 and Co50, for the two conditions concerning cementite for the liquidus and for an authorized appearance of cementite for the solidus. Indeed experimental values are about 50°C above the calculated liquidus and about 50°C below the calculated solidus. Suspending cementite does not change the results for liquidus but induce a significant improvement for the calculated solidus of Co45 and Co50. Concerning these two alloys Co45 and Co50 one can notice that, according to the DTA measurements, the alloys would have been partially melted during the aging at 1200°C (with solidification of the molten part during cooling) with probably some consequences for their microstructures.

3.6. Hardness measurements

Vickers indentations were performed on the heat-treated alloys. This was done several times per sample, always in an area close to the center of the initial ingot. Table 3 presents the obtained average values and the standard deviations. One can first notice that the dispersion of the results is significant in some cases, as revealed by a standard deviation of several tens of hardness points. Second, globally, for the alloys not really affected by the heat-treatment (stage temperature of 1000 or 1100°C) the hardness is of a high level, around 500-650 Hv. For a given heat-treatment hardness does not really depend on the carbon content. In contrast but an increase in temperature tends to lower hardness, as well as the presence of graphite. However, even after 50 hours spent at 1200°C, the hardness of the concerned alloys remains at a high level (450-500 Hv).

4. Discussion

The enrichment in carbon of the {Co-30wt.%C}-base beyond 2wt.% leads to alloys containing more carbides, which are still Cr_7C_3 without any change for a new stoichiometry richer in carbon (Cr_3C_2 for example). A new phase also appeared for the highest carbon contents: graphite. This graphite, present in small quantity, presents a shape which looks like the rosettes of lamellar graphite usually observed in solidified gray cast irons and which result from the eutectic {austenite+graphite}cells precipitation during solidification. Here the shape of graphite is blockier, maybe since graphite probably appeared in the present alloys essentially early during the post-solidification solid state cooling as suggested by Thermo-Calc in Fig. 8(b).

The carbon interval studied here led to hypo-eutectic alloys richer in {matrix + Cr_7C_3} eutectic compound than the alloys with less than 2wt.% previously studied [8], to an almost eutectic alloy (Co35) in which matrix dendrites are no longer present, and to hypereutectic alloys with coarse Cr_7C_3 carbides in addition to the eutectic Cr_7C_3 carbides. The total volume fraction of carbides thus reaches values considerably higher than those observed (about 20 vol.%) for the C-richest Co-30Cr-2C alloy studied in a previous work [8], since more than 50 vol.% of carbides (and even almost 60% with Co50) were obtained, although this rise in carbides volume fraction is limited by the precipitation of graphite.

Instead graphite Thermo-Calc predicted cementite for the Co35 to Co50 alloys, with notably very high quantities for the C-richest alloys (in Co50: more than 60 mass.% of cementite against less than 10 mass.% of Cr_7C_3). In the real alloys, after solidification as well as after the high temperature aging treatments, it is clear that graphite has really appeared and is thermodynamically stable (at least between 1000 and 1200°C). In addition, cementite was obviously absent in most of the observed microstructures. This phase was at least maybe present only in little quantities in the C-richest alloys as possibly revealed by very small additional peaks in the XRD spectra, and, in rare places, by local morphologies reminding the ledeburite ({austenite+cementite}-eutectic) of white cast irons.

Moreover, the agreement between real alloys and thermodynamic calculations (which is good for alloys with carbon content lower than 3.5) is significantly improved by suspending the cementite phase in the calculation conditions: presence of graphite,

calculated volume fractions of carbides consistent with measurements, and values of solidus temperatures closer to each other. However, for the Co45 and Co50 alloys, the calculated volume fractions of carbides (respectively graphite) are lower (resp. higher) than the measured surface fractions. This can be due to the appearance, in the real alloys, of a little quantity of cementite beside the Cr_7C_3 which remains the principal carbide present. This should lead to a small increase in carbides volume fraction and a small decrease in graphite fraction. Another reason is, for the Co45 and Co50 alloys aged at 1200°C, a partial remelting of some zones of the alloys which can thereafter disturb the microstructures. Thirdly it is also possible that, concerning only carbides, the particular shape of the pro-eutectic carbides leads to a non-respect of the equivalence of the surface fractions and the volume fractions, due to a dependence of the surface fraction on the orientation of these acicular carbides. This can affect the experiment-calculation comparisons, especially for the C-richest alloys which present a great part of such coarse elongated carbides.

It was also seen that the matrix of the aged samples are not wholly FCC but is divided in FCC and HCP areas although calculations showed that matrix is only FCC at 1000, 1100 and 1200°C. This was not seen during the SEM observations but revealed by the X-Ray Diffraction spectra. This is more the result of a partial allotropic change during cooling after the 50 hours aging, than a supplementary mismatch between experiments and calculations. Such phenomenon is usual and the short temperature range over which the allotropic transformation can be stated simply by thermal expansion analysis. Thermodynamic calculations can also give useful indications: according to Thermo-Calc this occurs near 400-500°C, as is to say a low temperature by comparison to the fusion temperatures of these alloys. It appears logical that the total transformation FCC $\rightarrow$ HCP predicted by calculations cannot be achieved for kinetic reasons.

The indentation tests first confirm that the presence of great quantities of carbides lead to a high level of hardness, but this one tends to decrease when the heat-treatment temperature increases. The value of carbide volume fraction is not the sole criterion to take in consideration since the presence of some graphite, even in small quantities, is obviously detrimental for this property. This phase is then to avoid, by limiting the carbon enrichment of these alloys, or maybe by adding more chromium to promote the formation of carbides instead graphite.

5. Conclusion

Cobalt alloys are often refractory (Co, with a fusion point of almost 1500°C, was chosen to be the base of some superalloys). They are also hard (intrinsic hardness higher than nickel or iron). Enriching them with high amounts of carbon, and of chromium which easily forms carbides and also brings the alloys a good resistance against high temperature corrosion, may lead to corrosion-resistant alloys with high levels of hardness and refractoriness. Such alloys particularly rich in carbon (at the same levels of near-eutectic cast irons) were here elaborated and characterized. Their microstructures are effectively rich in carbides and these ones may be even more present, in volume proportions, than the matrix itself. This leads to high levels of hardness (near 600Hv) and to a good wear resistance, even if friction stresses lead to high temperatures on long times in service (microstructures remain almost unchanged after 50h at 1200°C). But it

also appears that a smooth phase, graphite, is also able to appear for carbon contents near 5wt.%, which limits the increase in carbide fractions, but also leads to mechanically weakened zones. Such graphite particles, with near-lamellar shapes, can act as stress concentration sites, which is particularly dangerous in such alloys the impact toughness of which is probably very low. Another problem is the size of some of the pro-eutectic carbides which can be also detrimental for this property.

If the morphology of these carbides cannot be changed to a less detrimental one by an aging treatment, it is possible that the carbide fraction can be another time increased by adopting higher chromium contents, without appearance of graphite. This can be the subject of a new study.

Acknowledgements

The authors thank Moussa Ba and Ahmed Dia for their contribution, the Common Service of Microanalysis of the Faculty of Science and Technologies of the University Henri Poincaré Nancy 1 (Electron microscopy and microanalysis) and Pascal Villeger (XRD analyses).

References

[1] D. A. Bridgeport, W.A. Brandtley, and P. F. Herman, Cobalt-Chromium and Nickel-Chromium Alloys for Removable Prosthodontics, Part 1: Mechanical Properties, J. Prosthodontics, 1993, 2(3), p 144-150.

[2] C. T. Sims, W. C. Hagel, The Superalloys, John Wiley & Sons, New York, 1972.

[3] P. Berthod, J. L. Bernard, and C. Liébaut, Cobalt alloy and fabrication of articles from the alloy, Patent WO99/16919.

[4] B. Roebuck, and E. A. Almond, Deformation and Fracture Processes and the Physical Metallurgy of Tungsten Carbide-Cobalt Hardmetals, Int. Mat. Rev., 1988, 33(2), p 90-110.

[5] A.Klimpel, L.A. Dobrzanski, A. Lisiecki, and D.Janicki, The Study of Properties of Ni-W_2C and Co-W_2C Powders Thermal Sprayed Deposits, J. Mater. Proc. Technol., 2005, 164-165, p 1068-1073.

[6] G. V. Samsonov, Handbooks of High-Temperature materials N°2. Properties Index, Plenum Press, New York, 1964.

[7] D. Young, High Temperature Oxidation and Corrosion of Metals, Elsevier Corrosion Series, Oxford, 2008.

[8] P. Berthod, P. Lemoine, and J. Ravaux, High-Temperature Microstructures of Ternary Co-30wt.% Cr-based Alloys over the [0-2.0wt.%] Carbon Range, J. Alloys Compd, 2009, 467(1-2), p 227-234.

[9] Handbook of Chemistry and Physics, 57th edition, 1976-1977.

[10] Thermo-Calc version N: "Foundation for Computational Thermodynamics" Stockholm, Sweden, Copyright (1993, 2000). www.thermocalc.com

[11] A. Fernandez Guillermet, Critical Evaluation of the Thermodynamic Properties of Cobalt, Int. J. Thermophys., 1987, 8(4), p 481-510.

[12] J.-O. Andersson, Thermodynamic properties of chromium, Int. J. Thermophys., 1985, 6(4), p 411-419.

[13] P. Gustafson, An Evaluation of the Thermodynamic Properties and the P,T Phase Diagram of Carbon, Carbon, 1986, 24(2), p 169-176.

[14] A. Fernandez Guillermet, Thermodynamic Analysis of the Cobalt-Carbon System, Z. Metallkde, 1987, 78(10), p 700-709.

[15] J.-O. Andersson, Thermodynamic properties of chromium-carbon, Calphad, 1987, 11(3), p 271-276.

[16] A. Fernandez Guillermet, Thermodynamic Properties of the Iron-Cobalt-Carbon System, Z. Metallkde., 1988, 79(5), p 317-329.

Table 1
Thermo-Calc calculations without suspended phase: natures and mass fractions of the different phases present at 1000, 1100 and 1200°C for the targeted chemical compositions ("1": cementite authorized; "2": cementite suspended)
(matrix is of the {face centred cubic}–type for all alloys at all temperatures)

$\%_{mass}$	1000°C		1100°C		1200°C	
	Cr_7C_3	Cementite or Graphite	Cr_7C_3	Cementite or Graphite	Cr_7C_3	Cementite or Graphite
Co25	27.22	/	26.39	/	25.23	/
Co30	32.64	/	31.51	/	30.00	/
(1) Co35	34.59	4.67 (cem.)	31.82	6.68 (cem.)	30.86	5.58 (cem.)
(2) Co35	37.95	/	36.37	/	34.42	/
(1) Co40	25.97	23.94 (cem.)	23.75	25.53 (cem.)	23.17	24.32 (cem.)
(2) Co40	42.52	0.05 (**graph**)	40.31	0.06 (**graph**)	38.10	0.04 (**graph**)
(1) Co45	17.35	43.22 (cem.)	15.67	44.37 (cem.)	15.49	43.07 (cem.)
(2) Co45	42.55	0.55 (**graph**)	40.37	0.56 (**graph**)	38.17	0.54 (**graph**)
(1) Co50	8.73	62.50 (cem.)	7.60	63.21 (cem.)	7.81	61.81 (cem.)
(2) Co50	42.59	1.05 (**graph**)	40.43	1.06 (**graph**)	38.25	1.04 (**graph**)

(According to Thermo-Calc, the composition in mass of the cementite phase does not depend on the the carbon content in alloy but only on temperature: this is 58.78Co-34.57Cr-6.65C at 1200°C, 58.42Co-34.92Cr-6.66C at 1100°C and 58.28Co-35.06Cr-6.66C at 1000°C)

Table 2
Natures (XRD) and surface fractions (Image Analysis) of carbides in the Co25, Co30 and Co35 alloys heat-treated at 1000, 1100 and 1200°C (matrix is of the {face centred cubic}–type for three alloys at all temperatures); comparison with Thermo-Calc results (*: calculations performed with suspended cementite)

% vol.	1000°C		1100°C		1200°C	
Exp.	Cr_7C_3 (+ cem.?)	Graph.	Cr_7C_3 (+ cem.?)	Graph.	Cr_7C_3 (+ cem.?)	Graph.
Calc.	Cr_7C_3	Graph.	Cr_7C_3	Graph.	Cr_7C_3	Graph.
Exp.	27.0 ±0.9	/	36.3 ±2.5	/	27.9 ±1.8	/
Co25	Λ	=	V	=	=	=
Calc.	30.1	/	29.2	/	27.9	/
Exp.	37.9 ±1.3	/	45.0 ±1.1	/	28.1 ±1.9	0.1 ±0.2
Co30	V	=	**V V**	=	Λ	=
Calc.	35.8	/	34.6	/	33.0	/
Exp.	41.0 ±0.8	/	41.1 ±3.2	/	35.1 ±2.2	0.1 ±0.1
Co35*	=	=	=	=	Λ	=
Calc.	41.3	/	39.6	/	37.6	/

(=: calculated value in the experimental range, Λ or V : calc. value slightly higher or lower the experimental range, **Λ Λ** or **V V**: calc. value significantly higher or lower than the experimental range)

Table 3
Natures (XRD) and surface fractions (Image Analysis) of carbides in the Co40, Co45 and Co50 alloys heat-treated at 1000, 1100 and 1200°C (matrix is of the {face centred cubic}–type for three alloys at all temperatures); comparison with Thermo-Calc results (all calculations performed with suspended cementite)

% vol.	1000°C		1100°C		1200°C	
Exp.	Cr_7C_3 (+ cem.?)	Graph.	Cr_7C_3 (+ cem.?)	Graph.	Cr_7C_3 (+ cem.?)	Graph.
Calc.	Cr_7C_3	Graph.	Cr_7C_3	Graph.	Cr_7C_3	Graph.
Exp.	45.8 ±4.1	0.03 ±0.02	37.3 ±4.3	0.70 ±1.11	44.9 ±2.9	0.08 ±0.13
Co40	=	/\	/\	=	\/	=
Calc.	45.9	0.17	43.6	0.20	41.4	0.13
Exp.	58.0 ±4.7	0.45 ±0.24	30.1 ±2.8	0.08 ±0.05	53.4 ±5.7	0.10 ±0.17
Co45	**\/ \/**	**/\ /**	**/\ /**	**/\ /**	**\/ \/**	**/\ /**
Calc.	45.4	1.80	43.2	1.84	41.0	1.78
Exp.	51.2 ±2.4	2.20 ±1.15	35.5 ±6	0.13 ±0.14	59.4 ±10.1	0.14 ±0.15
Co50	**\/ \/**	/\	/\	**/\ /**	**\/ \/**	**/\ /**
Calc.	44.9	3.40	42.7	3.45	40.6	3.39

(=: calculated value in the experimental range, /\ or \/ : calc. value slightly higher or lower the experimental range, **/\ /** or **\/ \/**: calc. value significantly higher or lower than the experimental range)

Table 4. Hardness of the heat-treated alloys (Hv30kg)

% vol.	1000°C	1100°C	1200°C
Co25	640 ±36	539 ±3	472 ±21
Co30	623 ±33	584 ±36	449 ±29
Co35	635 ±6	570 ±9	483 ±12
Co40	558 ±5	562 ±22	Not done
Co45	478 ±3	425 ±18	
Co50	605 ±37	501 ±32	

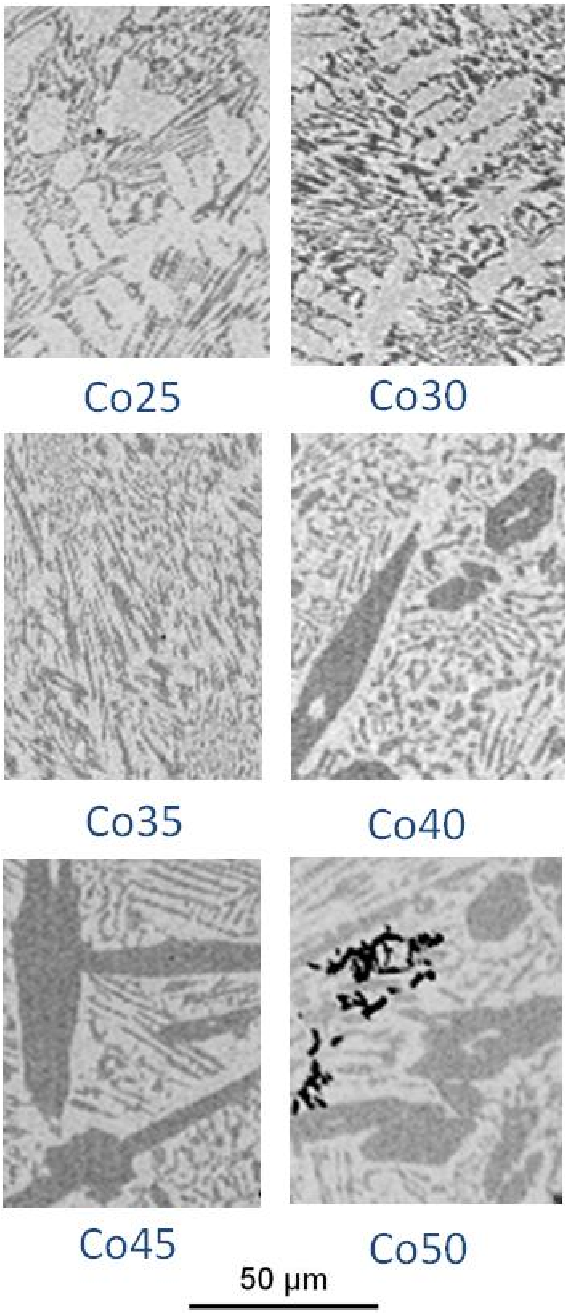

Fig. 1. Micrographs illustrating the as-cast microstructures of the studied alloys (SEM/BSE micrographs)

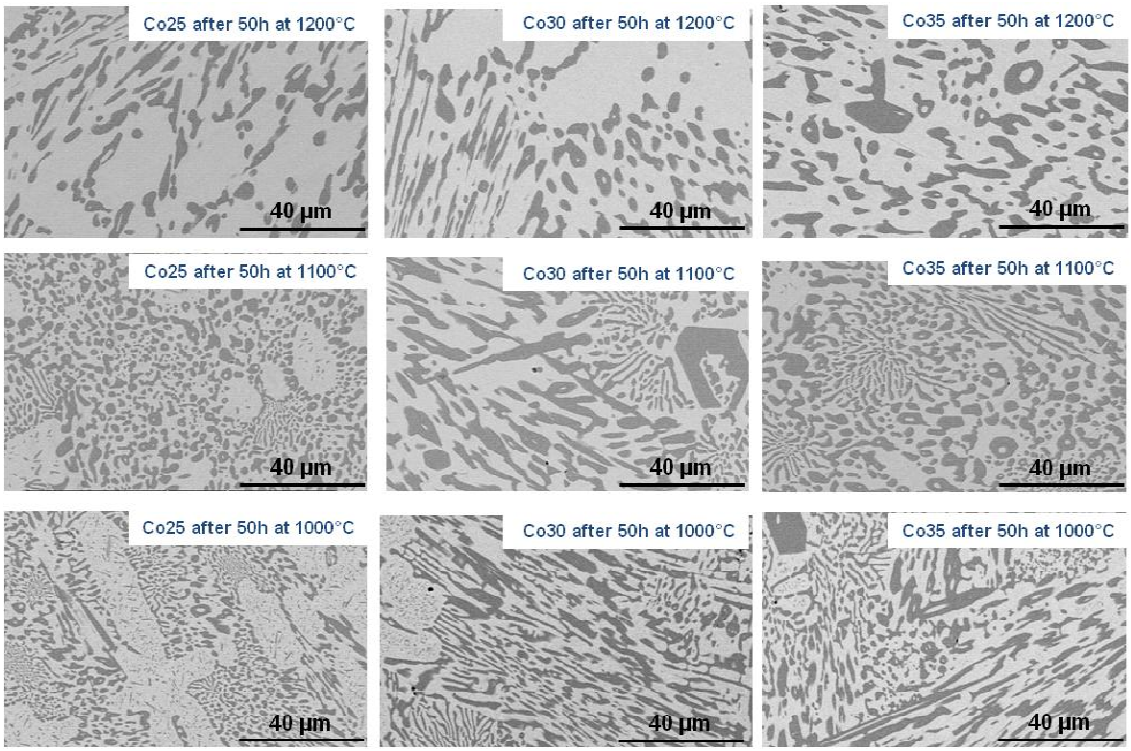

Fig. 2. Microstructures of the Co-30Cr-2.5 to 3.5C alloys after 50 hours at 1000, 1100 and 1200°C (SEM/BSE micrographs)

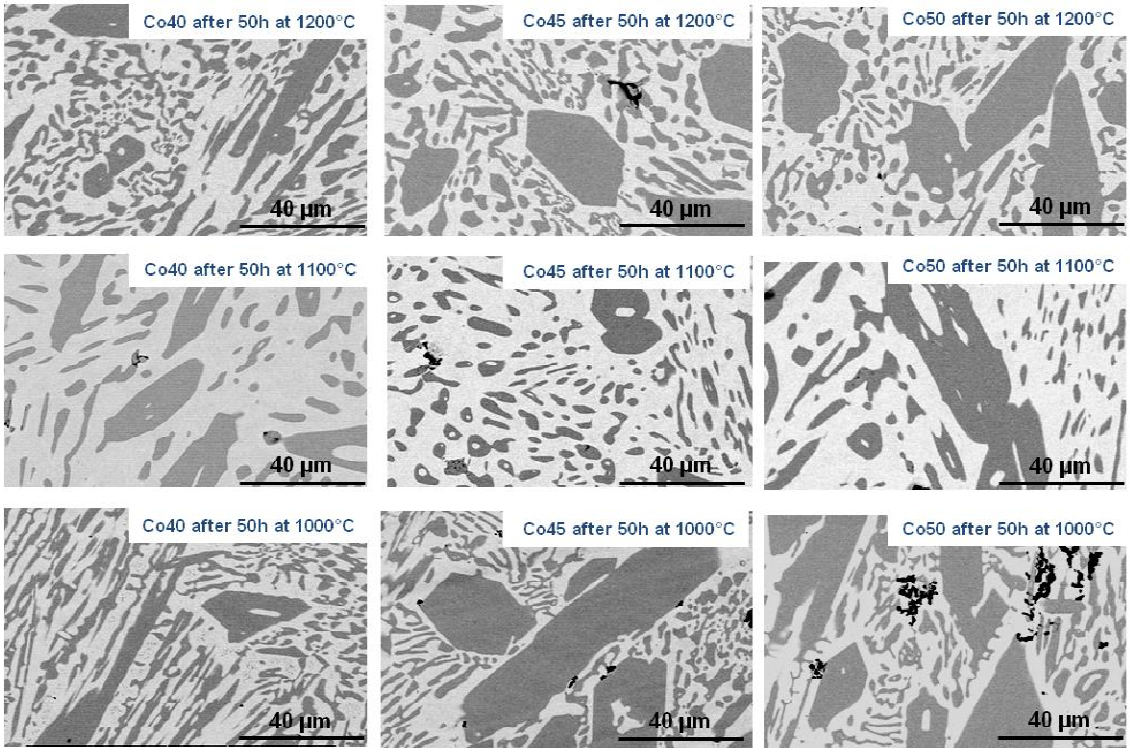

Fig. 3. Microstructures of the Co-30Cr-4.0 to 5.0C alloys after 50 hours at 1000, 1100 and 1200°C (SEM/BSE micrographs)

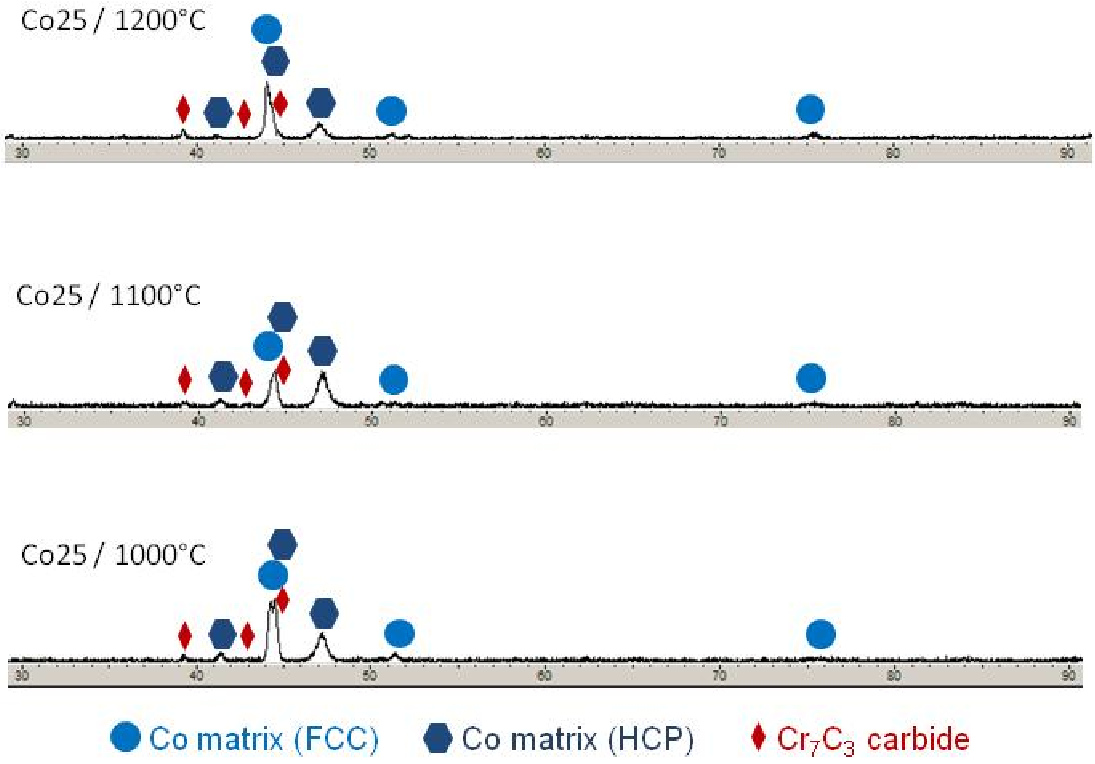

Fig. 4. XRD spectra obtained on three samples cut in the Co-30Cr-2.5C alloy and aged 50h at 1000, 1100 and 1200°C

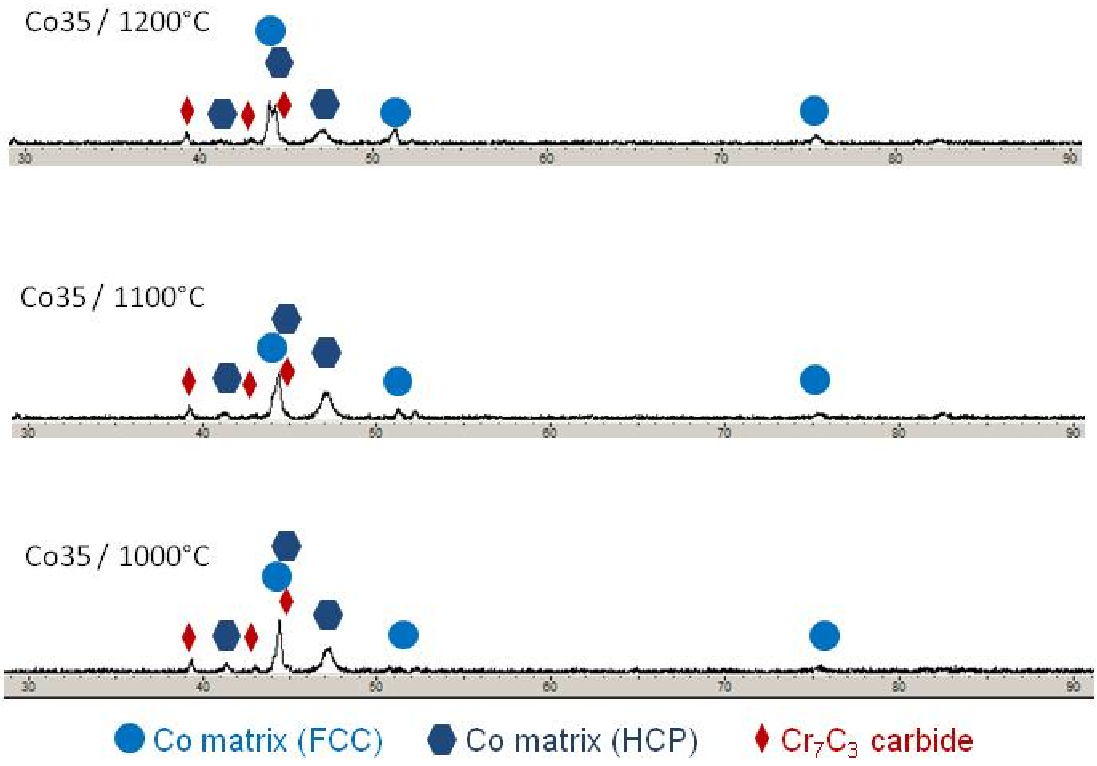

Fig. 5. XRD spectra obtained on three samples cut in the Co-30Cr-3.5C alloy and aged 50h at 1000, 1100 and 1200°C

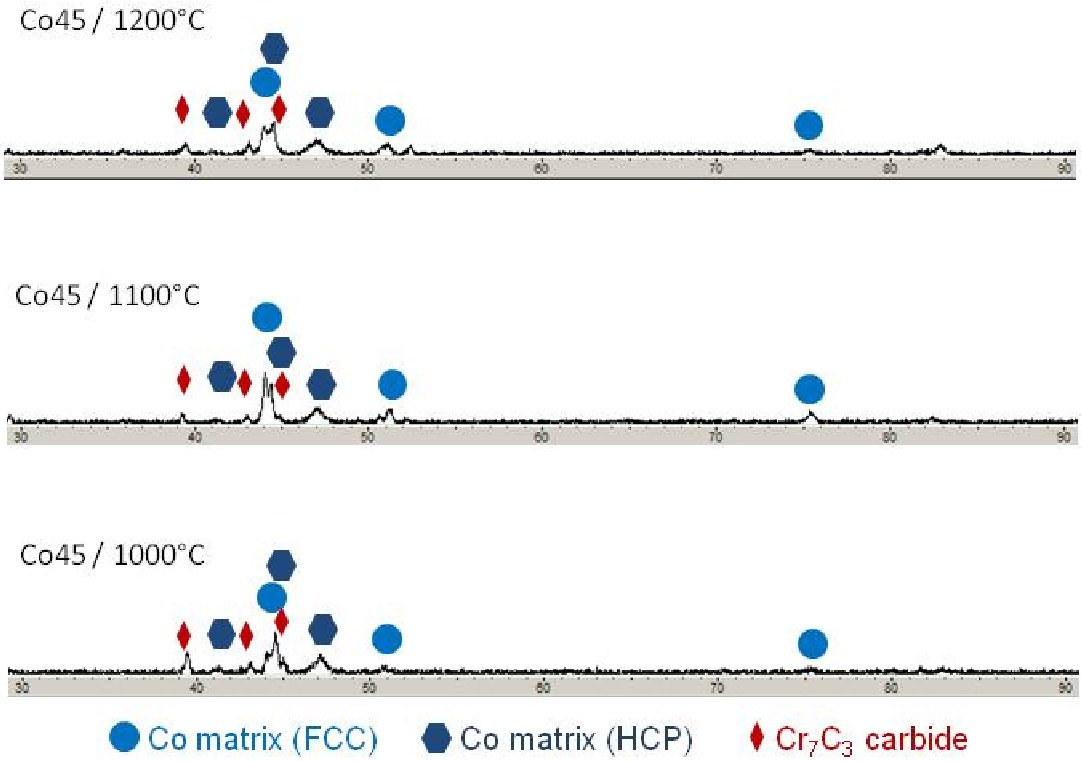

Fig. 6. XRD spectra obtained on three samples cut in the Co-30Cr-4.5C alloy and aged 50h at 1000, 1100 and 1200°C

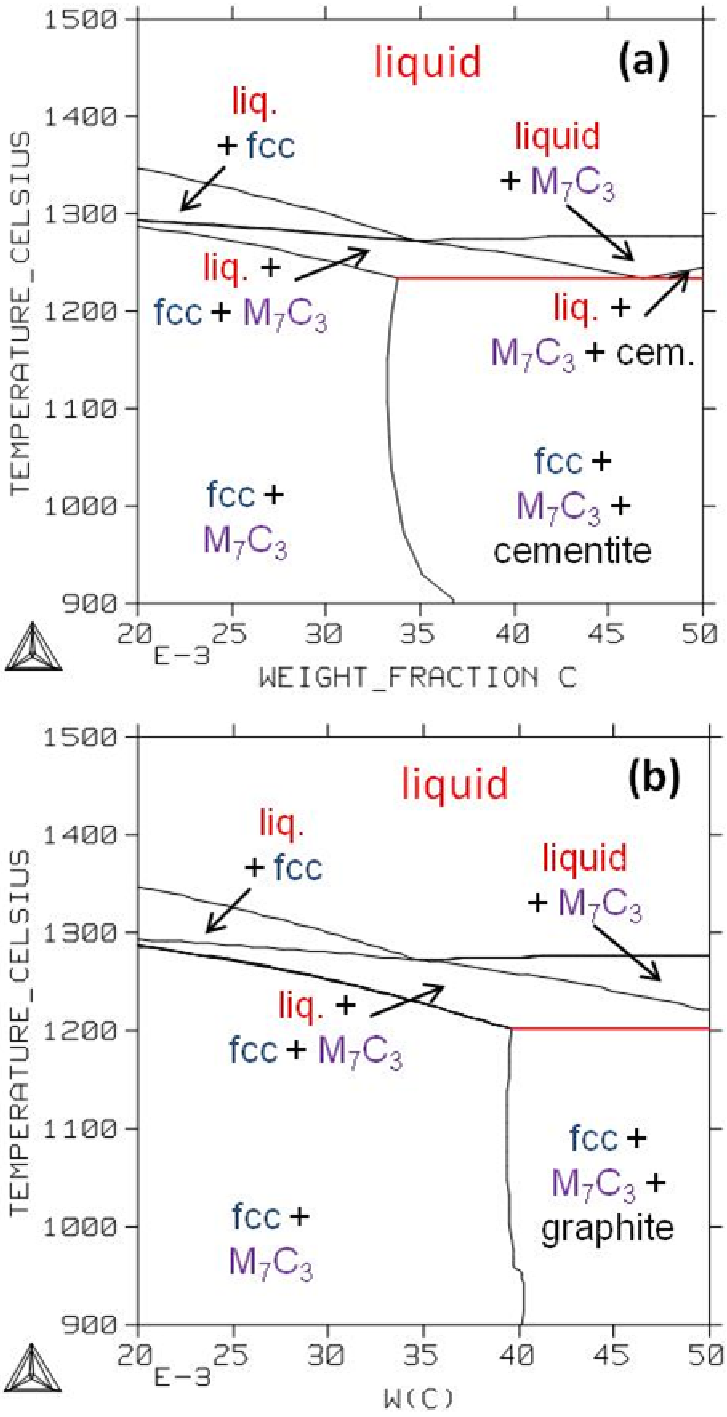

Fig. 7. 30wt.%C-sections of the Co-Cr-C diagrams between 2 and 5wt.%C computed by Thermo-Calc: (a) without condition applied to cementite,
(b) with cementite declared as suspended phase

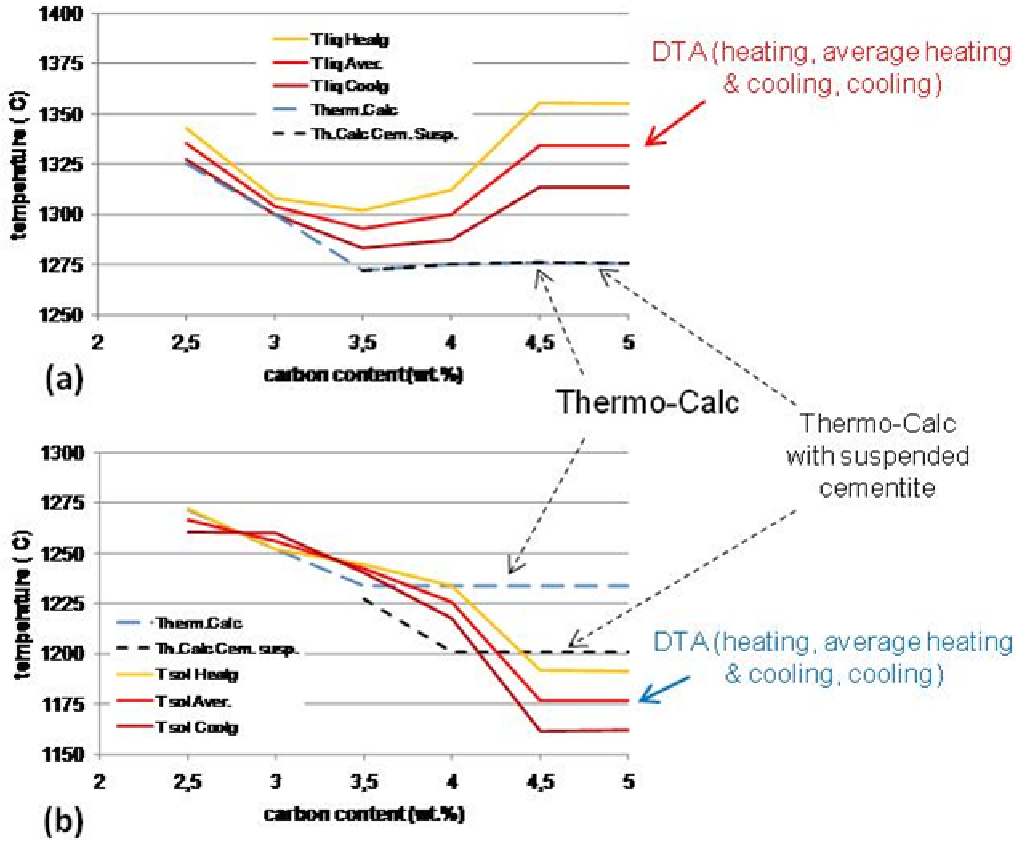

Fig. 8. Evolution vs. %C of the liquidus temperature (a) and of the solidus temperature (b) as experimentally determined, with comparison to Thermo-Calc results according to calculations performed without or with suspension of the cementite phase